Modeling groundwater responses to climate change in the Prairie Pothole Region

Zhe Zhang[1], Yanping Li[1*], Michael Barlage[2], Fei Chen[2], Gonzalo Miguez-Macho[3], Andrew Ireson[1], Zhenhua Li[1]

[1] *Global Institute for Water Security, University of Saskatchewan, Saskatoon, SK, Canada*

[2] *National Center for Atmospheric Research, Boulder, Colorado, USA*

[3] *Nonlinear Physic Group, Faculty of Physics, Universidade de Santiago de Compostela, Galicia, Spain*

Abstract

Shallow groundwater in the Prairie Pothole Region (PPR) is recharged predominantly by snowmelt in the spring and supplies water for evapotranspiration through the summer and fall. This two-way exchange is underrepresented in current land surface models. Furthermore, the impacts of climate change on the groundwater recharge rates are uncertain. In this paper, we use a coupled land and groundwater model to investigate the hydrological cycle of shallow groundwater in the PPR and study its response to climate change at the end of the 21st century. The results show that the model does a reasonably good job of simulating the timing of recharge. The mean water table depth (WTD) is well simulated, except the model predicts deep WTD in northwestern Alberta. The most significant change under future climate conditions occurs in the winter, when warmer temperature changes the rain/snow partitioning, delaying the time for snow accumulation/soil freezing while advancing early melting/thawing. Such changes lead to an earlier start to a longer recharge season, but with lower recharge rates. Different signals are shown in the eastern and western PPR in the future summer, with reduced precipitation and drier soils in the east but little change in the west. The annual recharge increased by 25% and 50% in the eastern and western PPR, respectively. Additionally, we found the mean and seasonal variation of the simulated WTD are sensitive to soil properties and fine-scale soil information is needed to improve groundwater simulation on regional scale.

Keywords: Groundwater, Recharge, Climate Change, Prairie Pothole Region, Hydrological Cycle,

Introduction

The Prairie Pothole Region (PPR) in North America is located in a semi-arid and cold region, where evapotranspiration (ET) exceeds precipitation (PR) in summer and near-surface soil is frozen in winter (Gray, 1970; Granger and Gray, 1989; Hayashi et al., 2003; Pomeroy et al., 2007; Ireson et al., 2013; Dumanski et al., 2015). These climatic conditions have introduced unique hydrological characters to the groundwater flow in the PPR (Ireson et al., 2013). During winters, frozen soils reduce permeability and snow accumulates on the surface, prohibiting infiltration (Niu and Yang 2006; Mohammed et al., 2018). At the same time, the water table slowly declines due to a combination of upward transport to the freezing front by the capillary effect and discharge to rivers (Ireson et al., 2013). In early spring, snowmelt becomes the dominant component of the hydrological cycle and the melt water runs over frozen soil, with little infiltration contributing to recharge. As the soil thaws, the increased infiltration capacity allows snowmelt recharge to the water table, the previously upward water movement by capillary effect to reverse and move downwards, and the water table to rise to its maximum level. In summer and fall, when high ET exceeds PR, capillary rise may draw water from the groundwater aquifers to supply ET demands, declining water table. These processes characterize the critical two-way water exchange between the unsaturated soils and saturated groundwater aquifers.

Previous studies have suggested that substantial changes to groundwater interactions with unsaturated soils are likely to occur under climate change (Tremblay et al., 2011; Green et al., 2011; Ireson et al., 2013, 2015). Existing modeling studies on the impacts of climate change on groundwater are either at global or basin/location-specific scales (Meixner et al., 2016). Global-level groundwater studies focus on potential future recharge trends (Doll and Fiedler, 2008; Doll, 2009; Green et al., 2011), yet coarse resolution analysis from global climate models (GCMs) provided insufficient specificity to inform decision making. Basin-scale groundwater studies connect the climate with groundwater-flow models to understand the climate impacts on specific systems (Maxwell and Kollet, 2008; Kurylyk and MacQuarrie, 2013; Dumanski et al., 2015). Regional groundwater modeling studies, such as in the Colorado River Basin (Christensen et al., 2004) and in the western U.S. (Niraula et al., 2017), have applied downscaled climate scenarios from GCMs to drive large scale hydrology models. These studies identified research gaps associated with poor representation of groundwater-soil interactions in models and uncertainties in future climate projections.

It is challenging to represent groundwater flows in LSMs because the important two-way water exchange between unsaturated soils and groundwater aquifers was neglected in previous LSMs. Recently, this two-way exchange has been implemented in coupled land surface – groundwater models (LSM-GW). For example, Maxwell and Miller (2005) used a groundwater model (ParFlow) coupled with the Common Land Model (CLM) as a single column model. They found that the coupled and uncoupled models were very similar in simulated sensible heat flux (SH), ET, and shallow soil moisture (SM), but differed greatly in simulated runoff and deep SM. Later on, Kollet and Maxwell (2008) incorporated the ET effect on redistributing moisture upward from shallow water table depth (WTD) and found the surface energy partitioning is highly sensitive to the WTD when the WTD is less than 5 m below ground surface. Niu et al. (2011) implemented a simple groundwater model (SIMGM, Niu et al., 2007), into the community Noah LSM with multi-parameterization options (Noah-MP LSM), by adding an unconfined aquifer at the bottom of soil layers. More complex features such as three-dimensional subsurface flow and two-dimensional surface were included in ParFlow v3 and evaluated over much of continental North America for a very fine 1-km resolution (Maxwell et al., 2015). These recent development in coupled land and groundwater models have advanced our knowledge on the important interactions between soil and groundwater aquifer.

In cold regions, soil freeze-thaw processes further complicate this two-way exchange. Field studies have found that frozen soil not only influences the timing and amount of downward recharge to aquifers by reducing the soil permeability (Koren et al., 1999; Niu et al., 2006; Kelln et al., 2007), but may also induce upward water transport from aquifers to soil freezing fronts (Spaans and Baker, 1996; Remenda et al., 1996; Hansson et al., 2004). In the modeling community, a range of approaches have been applied to deal with frozen soil parameterizations. Earlier LSMs assumed no significant heat transfer and soil water redistribution for sub-freezing temperature, for example, in simplified SiB and BATS (Xue et al., 1991; Dickinson et al., 1993; Niu and Zeng, 2012). Koren et al. (1999) suggested that the frozen soil is permeable due to macropores that exist in soil structural aggregates, such as cracks, dead root passages, and worm holes. The NoahV3 model adopted this scheme as its default option. Niu and Yang (2006) suggested to separate a model grid into frozen and unfrozen patches, and these two patches have a linear effect on the soil hydraulic properties. This treatment was incorporated into CLM 3.0 and Noah-MP in 2007 and 2011, respectively.

The spatial heterogeneity of soil moisture and WTD requires high-resolution meteorological input that direct outputs from GCMs are too coarse to provide. In GCMs, differences in simulated precipitation stem from the choice of convection parameterization scheme (Sherwood et al., 2014;

Prein et al., 2015). An important approach to improve precipitation simulation is to conduct dynamical downscaling using the convection-permitting model (CPM) (Ban et al., 2014; Prein et al., 2015; Liu et al., 2017). The CPM uses a high spatial resolution (usually under 5-km) to explicitly resolve convection without activating convection parameterization schemes. CPMs can also improve the representation of fine-scale topography and spatial variations of surface fields (Prein et al., 2013). These CPM added-values provide an excellent opportunity to investigate water table dynamics in the PPR.

The objectives of this paper are to 1) investigate the performance of a regional scale coupled land-groundwater model in simulating groundwater water levels, recharge and storage in a seasonally frozen environment in PPR; and 2) explore the possible impacts of climate change on these processes.

In this paper, we use a physical process-based LSM (Noah-MP) coupled with a groundwater dynamics model (MMF model). The coupled Noah-MP-MMF model is driven by two sets of meteorological forcing for 13 years under current and future climate scenarios. These two sets of meteorological dataset are from a CPM dynamical downscaling project using the Weather Research & Forecast (WRF) model with 4-km grid spacing covering the Contiguous U.S. and Southern Canada (WRF CONUS, Liu et al., 2017). The paper is structured as follows: Section 2 introduces the groundwater observations for WTD evaluation in the PPR, the coupled Noah-MP-MMF model, and the meteorological forcing from the WRF CONUS project. Section 3 evaluates the model simulated WTD timeseries and shows the groundwater budget and hydrological changes due to climate change. Section 4 and 5 offer a broad discussion and conclusion.

2. Data and Methods

2.1 Observational data

Groundwater observation data were obtained through several agencies: (1) the United States Geological Survey (USGS) National Water Information System in the U.S. (https://waterdata.usgs.gov/nwis/gw), (2) the Alberta Environment (http://aep.alberta.ca/water/programs-and-services/groundwater/groundwater-observation-well-network/default.aspx), (3) the Saskatchewan Water Security Agency (https://www.wsask.ca/Water-Info/Ground-Water/Observation-Wells/).

Initially, groundwater data from 160 wells were acquired, 72 in the U.S., 43 from Alberta, and 45 from Saskatchewan. We used the following criteria to select qualified stations for our study and evaluate our model performance against these observations:

1) the location of the wells are within the PPR region;
2) a sufficiently long data record exists during the simulation period. We define the observation availability as the available observation period within the 13-year simulation period and select wells with observation availability greater than 80%;
3) we only take data from unconfined aquifers with shallow groundwater levels (mean WTD > 5 m);
4) we only take data with minimal anthropogenic effects (such as from pumping or irrigation).

These criteria reduced the observation data to 33 well records, with six in Alberta, 13 in Saskatchewan and 14 from the U.S. **Table 1** summarizes the information for each selected well, and **Fig. 1**(a) shows the location of the wells in our study area. It is noteworthy that most of the groundwater sites have more permeable deposits (sand and gravel) as provincial and state agencies don't monitor low permeability formations. More information about the selecting criteria are provided in the supplemental materials.

Fig. 1 (a) Topography of the Prairie Pothole Region (PPR) and station location of rain gauges (black dots) and groundwater wells (red diamonds); (b) Topography of the WRF CONUS domain, with the black box indicating the PPR domain.

Table 1. Summary of the locations and aquifer type and soil type of the 33 selected wells.

2.2 Groundwater and Frozen Soil Scheme in Noah-MP

In the present study, we used the community Noah-MP LSM (Niu et al. 2011; Yang et al. 2011), coupled with a GW model – the MMF model (Fan et al. 2007; Miguez-Macho et al., 2007). This coupled model has been applied in many regional hydrology studies in offline mode (Miguez-Macho and Fan 2012; Martinez et al., 2016) and coupled with regional climate models (Anyah et al., 2008; Barlage et al., 2015). We present here a brief introduction to the MMF groundwater scheme and the frozen soil scheme in Noah-MP, further details can be found in previous studies (Fan et al., 2007;Miguez-Macho et al., 2007; Niu and Yang, 2006).

Fig. 2 is a diagram of the structure of 4 soil layers (0.1, 0.3, 0.6 and 1.0 m) and the underlying unconfined aquifer in Noah-MP-MMF. The MMF scheme defines explicitly an unconfined aquifer below the 2-m soil and an auxiliary soil layer stretching to the WTD, which varies in space and time [m]. The thickness of this auxiliary layer (z_{aux} [m]) is also variable, depending on the WTD:

$$z_{aux} = \begin{cases} 1, & WTD \geq -3 \\ -2 - WTD, & WTD < -3 \end{cases} \qquad (1)$$

The vertical fluxes include gravity drainage and capillary flux, solved from the Richards' equation,

$$q = K_\theta \left(\frac{\partial \psi}{\partial z} - 1\right), \qquad K_\theta = K_{sat} * \left(\frac{\theta}{\theta_{sat}}\right)^{2b+3}, \quad \psi = \psi_{sat} * \left(\frac{\theta_{sat}}{\theta}\right)^{b} \quad (2)$$

where q is water flux between two adjacent layers [m/s], K_θ is the hydraulic conductivity [m/s] at certain soil moisture content θ [m^3/m^3], ψ is the soil matric potential [m] and b is soil pore size index. The subscript *sat* denotes saturation. The recharge flux from/to the layer above WTD, R, can be obtained according to WTD:

$$R = \begin{cases} K_k * \left(\dfrac{\psi_i - \psi_k}{z_{soil(i)} - z_{soil(k)}} - 1\right), & WTD \geq -2 \\ K_{aux} * \left(\dfrac{\psi_4 - \psi_{aux}}{(-2) - (-3)} - 1\right), & -2 > WTD \geq -3 \\ K_{sat} * \left(\dfrac{\psi_{aux} - \psi_{sat}}{(-2) - (WTD)} - 1\right), & WTD < -3 \end{cases} \quad (3)$$

In the first case, WTD is in the resolved soil layers and z_{soil} is the depth of soil layer with the subscript k indicating the layer containing WTD while i is the layer above. The calculated water table recharge is then passed to the MMF groundwater routine.

The change of groundwater storage in the unconfined aquifer considers three components: recharge flux (R), river discharge (Q_r), and lateral flows (Q_{lat}):

$$\Delta S_g = (R - Q_r + \sum Q_{lat}) \quad (4)$$

where S_g [mm] is groundwater storage, Q_r [mm] is the water flux of groundwater-river exchange, and $\sum Q_{lat}$ [mm] are groundwater lateral flows to/from all surrounding grid cells. The groundwater lateral flow ($\sum Q_{lat}$) is the total horizontal flows between each grid cell and its neighbouring grid cells, calculated from Darcy's law with the Dupuit–Forchheimer approximation (Fan and Miguez-Macho 2010), as:

$$Q_{lat} = wT\left(\frac{h - h_n}{l}\right) \quad (5)$$

where w is the width of cell interface [m], T is the transmissivity of groundwater flow [m^2/s], h and h_n are the water table head [m] of local and neighboring cell, and l is the length [m] between cells. T depends on hydraulic conductivity K and WTD:

$$T = \begin{cases} \int_{-\infty}^{h} K\, dz & WTD \geq -2 \\ \int_{-\infty}^{(z_{surf}-2)} K\, dz \; + \sum K_i * \; dz_i & WTD < -2 \end{cases} \quad (7)$$

For $WTD < -2$, K is assumed to decay exponentially with depth, $K = K_4 \exp{(-z/f)}$, K_4 is the hydraulic conductivity in the 4-th soil layer and *f* is the e-folding length and depends on terrain slope. For WTD ≥ -2, *i* represents the number of layers between the water table and the 2-m bottom and z_{surf} is the surface elevation.

The river flux (Q_r) is also represented by a Darcy's law–type equation, where the flux depends on the gradient between the groundwater and the river depth and the riverbed conductance:

$$Q_r = RC \cdot (h - z_{river}) \quad (8)$$

with z_{river} is the depth of river [m] and *RC* is dimensionless river conductance, which depends on the slope of the terrain and equilibrium water table. Eq. (8) is a simplification which uses z_{river} rather than the water level in the river and, for this study, we only consider one-way discharge from groundwater to rivers. Finally, the change of WTD is calculated as the total fluxes fill or drain the pore space between saturation and the equilibrium soil moisture state (θ_{eq} [m^3/m^3]) in the layer containing WTD:

$$\Delta \mathrm{WTD} = \frac{\Delta S_g}{(\theta_{sat} - \theta_{eq})} \quad (9)$$

If ΔS_g is greater than the pore space in the current layer, the soil moisture content of current layer is saturated and the WTD rises to the layer above, updating the soil moisture content in the layer above as well. Vice versa for negative ΔS_g as water table declines and soil moisture decreases.

Fig. 2 Structure of the Noah-MP LSM coupled with MMF groundwater scheme, the top 2-m soil of 4 layers whose thicknesses are 0.1, 0.3, 0.6 and 1.0 m. An unconfined aquifer is added below the 2-m boundary, including an auxiliary layer and the saturated aquifer. Positive flux of *R* denotes downward transport. Two water table are shown, one within the 2-m soil and one below, indicating that the model is capable to deal with both shallow and deep water table.

There are two options in Noah-MP LSM for frozen soil permeability; option 1, the default option in Noah-MP, is from Niu and Yang (2006) and option 2 is inherited the Koren et al. (1999) scheme from NoahV3. Option 1 assumes that a model grid cell consists of permeable and impermeable patches and the area weighted sum of these patches gives the grid cell soil hydraulic properties. Thus, the total soil moisture (θ) in the grid cell is used to compute hydraulic properties as:

$$\theta = \theta_{ice} + \theta_{liq} \qquad (10)$$

$$K = \left(1 - F_{frz}\right)K_u = \left(1 - F_{frz}\right)K_{sat}\left(\frac{\theta}{\theta_{sat}}\right)^{2b+3} \quad (11)$$

the subscript *frz* and *u* denote the frozen and unfrozen patches in the grid point. The impermeable frozen soil fraction is parameterized as:

$$F_{frz} = e^{-\alpha(1-\theta_{ice}/\theta_{sat})} - e^{-\alpha} \qquad (12)$$

α = 3.0 is an adjustable parameter. The amount of the liquid water in soil layer is either θ_{liq} or $\theta_{liq,max}$, the maximum amount of liquid water, which is calculated by a more general form of the freezing-point depression equation:

$$\theta_{liq,max} = \theta_{sat}\left\{\frac{10^3 L_f\left(T_{soil} - T_{frz}\right)}{g T_{soil}\psi_{sat}}\right\}^{-\frac{1}{b}} \qquad (13)$$

where T_{soil} and T_{frz} are soil temperature and freezing point [K]; L_f is the latent heat of fusion [J kg^{-1}]; g is gravitational acceleration [m s^{-2}].

On the other hand, the option 2 uses only the liquid water volume to calculate hydraulic properties and assumes a non-linear effect of frozen soil on permeability. Also, the option 2 uses a variant of freezing-point depression equation with an extra term, $(1 + 8\theta_{ice})^2$, to account for the increased interface between soil particles and liquid water due to the increase of ice crystals. Generally, option 1 assumes that soil ice has a smaller effect on infiltration and simulates more permeable frozen soil than option 2 (Niu et al., 2011). For this reason, the option 1 allows the soil water to move and redistribute more easily within the frozen soil and we decide to use option 1 in our study.

2.3 Forcing Data

The output from the WRF CONUS dataset (Liu et al. 2017) are used as meteorological forcing to drive the Noah-MP-MMF model. The WRF CONUS project consists of two simulations. The first simulation is referred as the current climate scenario, or control run (CTRL), from Oct 2000 to Sep 2013, and forced with the 6-hourly 0.7° ERA-Interim reanalysis data. The second simulation is a perturbation to reflect the future climate scenario, closely following the pseudo global warming (PGW) approach in previous works (Rasmussen et al., 2014). The PGW simulation is forced with 6-hourly ERA-Interim reanalysis data plus a delta climate change signal derived from an ensemble of CMIP5 models under the RCP8.5 emission scenario and reflects the climate change signal between the end of 21^{st} and 20^{th} century.

Fig. 3 shows the annual precipitation in the PPR from 4-km WRF CONUS from the current climate and 32-km North America Regional Reanalysis (NARR, another reanalysis dataset commonly used for land surface model forcing). Both datasets show similar annual precipitation pattern and bias patterns compared to observations: underestimating of precipitation in the east and overestimating in the west. However, the WRF CONUS shows significant improvement of percentage bias in precipitation ((Model-Observation)/Observation) over the western PPR. For the consistency of the same source of data for current and future climate, the WRF-CONUS is the best available dataset for the coupled land-groundwater study in the PPR.

Fig. 3 Evaluation of the annual precipitation from WRF CONUS (top) and NARR (bottom) against rain gauge observation.

For the future climate study, the precipitation and temperature of the PGW climate forcing are shown in **Fig. 4** and **Fig. 5**. The WRF CONUS projects more precipitation in the PPR, except in the southeast of the domain in summer, where it shows a precipitation reduction of about 50 to 100 mm. On the other hand, the WRF CONUS projects strongest warming occurring in the northeast PPR in winter (**Fig. 5**), about 6–8 °C. Another significant warming signal occurs in summer in the southeast of domain, corresponding to the reduction of future precipitation, as seen in **Fig. 4**.

Fig. 4 Seasonal accumulated precipitation from current climate scenario(CTRL), future climate scenario (PGW) and projected change (PGW-CTRL) in the forcing data.

Fig. 5 Seasonal averaged temperature from CTRL, PGW, and the projected change (PGW-CTRL).

2.4 Model Setup

The two Noah-MP-MMF simulations representing the current climate and future climate are denoted as CTRL and PGW, respectively. The initial groundwater levels are from a global 1-km equilibrium groundwater map (Fan et al., 2013) and the equilibrium soil moisture for each soil layer is calculated at the first model timestep with climatology recharge, spinning up for 500 years. Since the model domain is at a different resolution than the input data, the appropriate initial WTD at 4-km may be different than the average at 1-km. To properly initialize the simulation, we spin up the model using the forcing of current climate (CTRL) for the years from 2000 to 2001 repeatedly (in total 10 loops).

Due to different data sources, the default soil types along the boundary between the U.S. and Canada are discontinuous. Thus, we use the global 1-km fine soil data (Shangguan et al., 2014, http://globalchange.bnu.edu.cn/research/soilw) in our study region. The soil properties for the aquifer use the same properties as the lowest soil layer from the Noah-MP 2-m soil layers.

3. Results

3.1 Comparison with groundwater observations

According to the locations of 33 groundwater wells in **Table 1**, the simulated WTD from the closest model grid points are extracted. **Fig. 6** shows the modeled WTD bias from the CTRL run. We also select the monthly WTD timeseries from 8 sites, the observation are in black dots and CTRL in blue lines. See supplemental materials for the timeseries of 33 sites. The model produces reasonable values of mean WTD, the mean bias are smaller than 1 m in most of sites, except in Alberta, where the model predicts deep bias about 5 m in the northwestern part of PPR. The model also successfully captures the annual cycle of WTD, which rises in spring and early summer, because of snowmelt and rainfall recharge, and declines in summer and fall, because of high ET, and in winter because of frozen near-surface soil. In all observations, the timing of the water table rising and dropping is well simulated, as the timing and amount of infiltration and recharge in spring is controlled by the freeze-thaw processes in seasonally frozen soil.

Fig. 6. WTD (m) bias from CTRL simulation and timeseries from 8 groundwater wells in PPR (black for observation and blue for CTRL model simulation). See Table 2 CTRL column for the model statistics and supplemental materials for complete timeseries from 33 wells.

On the other hand, the model simulated WTD seasonal variation is smaller than observations. The small seasonal variation could be due to the misrepresentation between the lithology from the observational surveys and the soil types in the model grids. As mentioned in Section 2.2, the groundwater aquifer uses the same soil types as the bottom layer of the resolved 2-m soil layers. While sand and gravel are the dominant lithology in most of the sites, they are mostly clay and loam in the model (Table 1). For sandy soil reported in most of the sites, small capacity and fast responses to infiltration lead to large water table fluctuations, whereas, in the model, clay and loam soil allows low permeability and large capacity, and smoothens responses to recharge and capillary effects. Furthermore, the 4-layer soils are vertically homogeneous in soil type and the groundwater model uses the lowest level soil type as the aquifer lithology. For many part of the PPR, where groundwater level are perched at the top 5-m due to a layer called glacial till. These geohydrological characteristics cannot be reflected in this model and contribute to the deep WTD bias simulated in Alberta. This shortcoming of the model was also reported in a study taken place in the Amazon rainforest (Miguez-Macho et al., 2012).

3.2 Climate change signal in Groundwater fluxes

The MMF groundwater model simulates three components in the groundwater water budget, the recharge flux (R), lateral flow (Q_{lat}), and discharge flux to rivers (Q_r). Because the topography is usually flat in the PPR, the magnitude of groundwater lateral transport is very small (Q_{lat} less than 5 mm per year). On the other hand, the shallow water table in the PPR region is higher than the local river bed, thus, the Q_r term is always discharging from groundwater aquifers to rivers. As a result, the recharge term is the major contributor to the groundwater storage in the PPR, and its variation (usually between -100 to 100 mm) dominates the timing and amplitude of the water table dynamics. The seasonal accumulated total groundwater fluxes in the PPR (R+$Q_{lat} - Q_r$) are shown in **Fig. 7**. The positive (negative) flux in blue (red) means the groundwater aquifer is gaining (losing) water, causing the water table to rise (decline).

Fig. 7 Seasonal accumulated total groundwater fluxes (R+) for current climate (CTRL, top), future climate (PGW, middle) and projected change (PGW-CTRL, bottom) in forcing data. Black dashed lines in PGW-CTRL separate the PPR into eastern and western halves.

Under current climate conditions, the total groundwater fluxes show strong seasonal fluctuations, consistent with the WTD timeseries shown in **Fig. 6**. On average, in fall (SON) and winter (DJF), there is a 20-mm negative recharge, driven by the capillary effects and drawing water from aquifer to dry soil above. Spring (MAM) is usually the season with a strong positive recharge because snowmelt provides a significant amount of water, and soils thawing allow infiltration. The large amount of snowmelt water contributes to more than 100 mm of positive recharge in the eastern domain. It is until summer (JJA), when strong ET depletes soil moisture and results in about 50 mm of negative recharge.

Under future climate conditions, the increased PR in fall and winter leads to wetter upper soil layers, resulting in a net positive recharge flux (PGW – CTRL in SON and DJF). However, the PGW summer is impacted by increased ET under a warmer and drier climate, due to higher temperature and less PR. As a result, the groundwater uptake by the capillary effect is more critical in the future summer. Furthermore, there is a strong east-to-west difference in the total groundwater flux change from PGW to CTRL. In the eastern PPR, the change in total groundwater flux exhibits obvious seasonality while the model projects persistent positive groundwater fluxes in the western PPR.

3.3 Water budget analysis

Fig. 8 and **Fig. 9** show the water budget analysis for the eastern and western PPR (divided by the dotted line in 103° W in Fig. 7), respectively. Four components are presented in the figures, i.e. (1) PR and ET; (2) surface and underground runoff (*SFCRUN* and *UDGRUN*); and surface snowpack; (3) the change of soil moisture storage and (4) groundwater fluxes and the change of storage. In the current and future climate, these budget terms are plotted in annual accumulation ((a) and (b) for CTRL and PGW), whereas their difference are plotted in each month individually ((c) for PGW-CTRL).

Under current climate conditions, during snowmelt infiltration and rainfall events, water infiltrates into the top soil layer, travels through the soil column and exits the bottom of the 2-m boundary, hence, the water table rises. During the summer dry season, ET is higher than PR and the soil layers lose water through ET, therefore, the capillary effect takes water from the underlying aquifer and the water table declines. In winter, the near-surface soil in the PPR is seasonally frozen, thus, a redistribution of subsurface water to the freezing front results in negative recharge, and the water table declines.

In the eastern PPR, the effective precipitation (PR-ET) is found to increase from fall to spring, but decrease in summer in PGW (**Fig. 8**(1c)). Warmer falls and winters in PGW, together with increased PR, not only delay snow accumulation and bring forward snowmelt, but also change the precipitation partition – more as rain and less as snow. This warming causes up to 20 mm of snowpack loss (**Fig.8**(2c)). The underground runoff starts much earlier in PGW (December) (**Fig.8**(2b)) than in CTRL (February) (**Fig.8**(2a)). On the other hand, the warming in PGW also changes the partitioning of soil ice and soil water in unsaturated soil layers (**Fig**. 8(3c)). For late spring in PGW, the springtime recharge in the future is significantly reduced due to early melting and less snowpack remaining (**Fig. 8**(4c)). In the PGW summer, reduced PR (50 mm less) and higher temperatures (8 °C warmer) lead to reduction in total soil moisture, and a stronger negative recharge from the aquifer. Therefore, the increase of recharge from fall to early spring compensates the recharge reduction due to stronger ET in summer in the eastern PPR, and changes little in the annual mean groundwater storage (1.763 mm per year).

Fig. 8 Water budget analysis in the eastern PPR in (a) CTRL, (b) PGW and (c) PGW – CTRL. Water budget terms include: (1) *PR & ET*, (2) surface snow, surface runoff and underground runoff (*SNOW*, *SFCRUN*, and *UDGRUN*), (3) change of soil moisture storage (soil water, soil ice and total soil moisture, ΔSMC) and (4) groundwater fluxes and the change of groundwater storage (R, Q_{lat}, Q_r, ΔS_g). The annual mean soil moisture change (PGW-CTRL) is shown with black dashed line in (3). The Residual term is defined as *Res* = (R+Q_{lat}-Q_r)-ΔS_g in (4). Note that in (a) and (b) the accumulated fluxes and change in storage are shown in lines, whereas in (c) the difference in (PGW-CTRL) is shown for each individual month in bars.

These changes in water budget components in the western PPR (**Fig. 9**) are similar to those in the eastern PPR (**Fig. 8**), except in summer. The reduction in summer PR in the western the PPR (less than 5 mm reduction) is not as obvious as that in the eastern PPR (50 mm reduction) (**Fig. 4**). Thus, annual mean total soil moisture in future is about the same as in current climate (Fig. 9(3c)) and results in little negative recharge in PGW summer (**Fig. 9**(4c)). Therefore, the increase in annual recharge is more significant (10 mm per year), an increase of about 50% of the annual recharge in the current climate (20 mm per year) (**Fig. 9**(4c)).

Fig. 9 Same as Fig. 8. Water budget analysis in the **western PPR**: in (a) CTRL, (b) PGW and (c) PGW – CTRL. Water budget terms include: (1) *PR & ET*, (2) surface snow, surface runoff and underground runoff (*SNOW*, *SFCRUN*, and *UDGRUN*), (3) change of soil moisture storage (soil water, soil ice and total soil moisture, ΔSMC) and (4) groundwater fluxes and the change of groundwater storage (R, Q_{lat}, Q_r, ΔS_g). The annual mean soil moisture change (PGW-CTRL) is shown with black dashed line in (3). The Residual term is defined as $Res = (R+Q_{lat}-Q_r)-\Delta S_g$ in (4). Note that in (a) and (b) the accumulated fluxes and change in storage are shown in lines, whereas in (c) the difference in (PGW-CTRL) is shown for each individual month in bars.

In both the eastern and western PPR, the water budget components for the groundwater aquifer are plotted in **Fig. 8**(4) and **Fig. 9** (4), with the changes of each flux (PGW-CTRL) printed at the bottom. The groundwater lateral flow is a small term in areal average and has little impact on the groundwater storage. Nearly half of the increased recharge in both the eastern and western PPR is discharged to river flux (Q_r = 2.26 mm out of R = 4.15 mm in the eastern PPR and Q_r = 5.20 mm out of R = 10.72 mm in western PPR). Therefore, the groundwater storage change in the eastern PPR (1.76 mm per year) is not as great as that in the western PPR (5.39 mm per year).

These two regions of the PPR show differences in hydrological response to future climate because of the spatial variation of the summer PR. As shown in both **Fig. 4** (PGW-CTRL), **Fig. 8**(1) and **Fig. 9**(1), the reduction of future PR in summer in the eastern PPR is significant (50 mm). The spatial difference of precipitation changes in the PPR further results in the recharge increase doubling in the western PPR compared to the eastern PPR.

4. Discussion

4.1 Improving WTD Simulation

In Section 3.1, we show that the model is capable of simulating the mean WTD in most sites, yet predicts deep groundwater in Alberta and underestimates its seasonal variation. These results may be due to misrepresentations between model default soil type and the soil properties in the observational wells. To test this theory, an additional simulation, REP, is conducted by replacing the default soil types in the locations of these 33 groundwater wells with sand-type soil, which is the dominant soil types reported from observational surveys. The timeseries of the REP and default CTRL are shown in Fig. 10 (also see supplemental materials for the complete 33 sites) and a summary of the mean and standard deviation of the two simulations are provided in Table 2.

Fig. 10 Same as Fig. 6, WTD (m) bias from CTRL simulation and timeseries from 8 groundwater wells in PPR (black for observation and blue for CTRL model simulation, and red for the replacing soil type simulation). REP is the additional simulation by replacing the default soil type in the model with sandy soil type.

The REP simulation with sandy soil show two sensitive signals: (1) REP WTD are shallower than the default simulation; (2) and exhibit stronger seasonal variation. These two signals can be explained by the WTD equation in the MMF scheme:

$$\Delta WTD = \frac{\Delta(R + Q_{lat} - Q_r)}{(\theta_{sat} - \theta_{eq})} \quad (14)$$

Eq. (14) represents that the change of WTD in a period of time is calculated by the total groundwater fluxes, $\Delta(R + Q_{lat} - Q_r)$, divided by the available soil moisture capacity of current layer ($\theta_{sat} - \theta_{eq}$). In REP simulation, the parameters θ_{sat} for the dominant soil type in observational sites (sand/gravel) is smaller than those in default model grids (clay loam, sandy loam, loam, loamy sand, etc.). Therefore, changing the θ_{sat} is essentially reducing the storage in the aquifer and soil in this model grid. Given the same amount of groundwater flux, in the REP simulation, the mean WTD is higher and the seasonal variation is stronger than the default CTRL run.

In the REP simulation, we replaced soil type only at a limited number of sites because the geological survey data in high resolution and large area extent is not yet available for the whole PPR. At point scale, the WTD responses to climate change over these limited number of sites show diverse results and uncertainties (see supplemental materials). For the rest of the domain, the default soil type from global 1-km soil map is used. The REP modifications of soil types at point-scale have small contribution to the water balance analysis (Fig. 8 & 9) at regional-scale. Our results and conclusions for groundwater response to PGW doesn't change. We are currently undertaking a soil property survey project in the PPR region to obtain soil properties at high spatial resolution, both horizontal and vertical. This may provide better opportunity to improve WTD simulation as well as assess climate-groundwater interaction in future studies.

4.2 Climate Change Impacts on Groundwater Hydrological Regime

The warming and increased precipitation in cold seasons in future climate lead to later snow accumulation, higher recharge in winter and earlier melting in spring compared to current climate. Such changes in snowpack loss have been hypothesized in mountainous as well as high-latitude regions (Taylor et al 2013; Ireson et al., 2015; Meixner et al., 2016; Musselman et al., 2017). In addition to the amount of recharge, the shift of recharge season is also noteworthy. Under current climate conditions in spring, soil thawing (in March) is generally later than snowmelt (in February) by a month in the PPR. Thus, the snowmelt water in pre-thaw spring would either re-freeze after infiltrating into partially frozen soil or become surface runoff. Under the PGW climate, the warmer winter and spring allows snowmelt and soil thaw to occur earlier in the middle of winter (in January and February, respectively). As a result, the recharge season starts earlier in December, and last longer until June, results in longer recharge season but with lower recharge rate.

Future projected increasing evapotranspiration demand in summer desiccates soil moisture, resulting in more water uptake from aquifers to subsidize dry soil in the future summer. This groundwater transport to soil moisture is similar to the “buffer effect” documented in an offline study in the Amazon rainforest (Pokhrel et al., 2014). In , shallow water tables exist in the critical zone, where WTD ranges from 1 to 5 meters below surface and could exert strong influence on land energy and moisture fluxes feedback to the atmosphere (Kollet and Maxwell, 2008; Fan , 2015). Previous coupled atmosphere-land-groundwater studies at 30-km resolution showed that groundwater could support soil moisture during summer dry period, but has little impacts on precipitation in Central U.S. (Barlage et al., 2015). It would be an interesting topic to study the integrated impacts of shallow groundwater to regional climate in the convection permitting resolution (resolution < 5-km).

4.3 Fine-scale interaction between groundwater and Prairie pothole wetlands

Furthermore, groundwater exchange with prairie pothole wetlands are complicated and critical in the PPR. Numerous wetlands known as potholes or sloughs provide important ecosystem services, such as providing wildlife habitats and groundwater recharge (Johnson et al., 2010). Shallow groundwater aquifers may receive water from or lose water to prairie wetlands depending on the hydrological setting. Depression-focused recharge generated by runoff from upland to depression contributes to sufficient amount of water input to shallow groundwater (5-40 mm/year) (Hayashi et al., 2016).

On the other hand, groundwater lateral flow exchange center of a wetland pond to its moist margin is also an important component in the wetland water balance (van der Kamp and Hayashi, 2009; Brannen, et al., 2015; Hayashi et al., 2016). However, this groundwater-wetland exchange typically occurs on local scale (from 10 to 100 m) and thus, is challenging to represent in current land surface models or climate models (resolution from 1 km to 100 km). In this paper, we focus on the groundwater dynamics on regional scale, which is still unable to capture these small wetland features in this study. We admit this limitation and are currently developing a sub-grid scheme to represent small scale open water wetlands as a fraction within a grid cell and calculate its feedback to regional environments. Future studies on this topic will provide valuable insights on these key ecosystems and their interaction under climate change.

Conclusion

In this study, a coupled land-groundwater model is applied to simulate the interaction between the groundwater aquifer and soil moisture in the PPR. The climate forcing is from a dynamical downscaling project (WRF CONUS), which uses the convection-permitting model (CPM) configuration in high resolution. The goal of this study is to investigate the groundwater responses to climate change, and to identify the major processes that contribute to these responses in the PPR. To our knowledge, this is the first study applying CPM forcing in a hydrology study in this region. We have three main findings:

(1) the coupled land-groundwater model shows reliable simulation of mean WTD, however underestimates the seasonal variation of the water table against well observations. This could be attributed to several reasons, including misrepresentation of topography and soil types, as well as vertical homogenous soil layers used in the model. We further conducted an additional simulation (REP) by replacing the model default soil types with sand-type soil and the simulated WTDs were improved in both mean and seasonal variation. However, inadequacy of soil properties in deeper layer and higher spatial resolution is still a limitation.

(2) Recharge markedly increases due to projected increased PR, particularly from fall to spring under future climate conditions. Strong east-west spatial variation exists in the annual recharge increases, 25% in the eastern and 50% in the western PPR. This is due to the significant projected PR reduction in PGW summer in the eastern PPR but little change in the western PPR. This PR reduction leads to stronger ET demand, which draws more groundwater uptake due to the capillary effect, results in negative recharge in the summer. Therefore, the increased recharge from fall to

spring is consumed by ET in summer, and results in little change in groundwater in the eastern PPR, while gaining water in the western PPR.

(3) The timing of infiltration and recharge are critically impacted by the changes in freeze-thaw processes. Increased precipitation, combined with higher winter temperatures, results in later snow accumulation/soil freezing, partitioned more as rain than snow, and earlier snowmelt/soil thaw. This leads to substantial loss of snowpack, shorter frozen soil season, and higher permeability in soil allowing infiltration. Late accumulation/freezing and early melting/thawing leads to an early start of a longer recharge season from December to June, but with a lower recharge rate.

Our study has some limitations where future studies are encouraged:

(1) Despite the large number of groundwater wells in PPR, only a few are suitable for long-term evaluation, due to data quality, anthropogenic pumping, and length of data record. As remote sensing techniques advance, observing terrestrial water storage anomalies derived from the GRACE satellite may provide substantial information on WTD, although the GRACE information needs to be downscaled to a finer scale before comparisons can be made with regional hydrology models at km-scale (Pokhrel et al., 2013).

(2) This study is an offline study of climate change impacts on groundwater. It is important to investigate how shallow groundwater in the earth's critical zone could interact with surface water and energy exchange to the atmosphere and affect regional climate. This investigation would be important to the central North America region (one of the land atmosphere coupling "hot spots", Koster et al., 2004).

Acknowledgments

The authors Zhe Zhang, Yanping Li, Zhenhua Li gratefully acknowledge the support from the Changing Cold Regions Network (CCRN) funded by the Natural Science and Engineering Research Council of Canada (NSERC), as well as the Global Water Future project and Global Institute of Water Security at University of Saskatchewan. Yanping Li acknowledge the support from NSERC Discovery Grant. Fei Chen, Michael Barlage appreciate the support from the Water System Program at the National Center for Atmospheric Research (NCAR), USDA NIFA Grants 2015-67003-23508 and 2015-67003-23460, NSF INFEW/T2 Grant #1739705, and NOAA CFDA Grant #NA18OAR4590381. NCAR is sponsored by the National Science Foundation. Any opinions, findings, conclusions or recommendations expressed in this publication are those of the authors and do not necessarily reflect the views of the National Science Foundation.

Reference

Anyah, R. O., Weaver, C. P., Miguez-macho, G., Fan, Y. and Robock, A.: Incorporating water table dynamics in climate modeling : 3 . Simulated groundwater influence on coupled land-atmosphere variability, , 113, 1–15, doi:10.1029/2007JD009087, 2008.

Ban, N., Schmidli, J. and Schär, C.: Evaluation of the new convective-resolving regional climate modeling approach in decade-long simulations, J. Geophys. Res. Atmos., 119, 7889–7907, doi:10.1002/2014JD021478.Received, 2014.

Barlage, M., Tewari, M., Chen, F., Miguez-Macho, G., Yang, Z. L. and Niu, G. Y.: The effect of groundwater interaction in North American regional climate simulations with WRF/Noah-MP, Clim. Change, 129(3–4), 485–498, doi:10.1007/s10584-014-1308-8, 2015.

Brannen, R., Spence, C. and Ireson, A.: Influence of shallow groundwater-surface water interactions on the hydrological connectivity and water budget of a wetland complex, Hydrol. Process., 29(18), 3862–3877, doi:10.1002/hyp.10563, 2015.

Christensen NS, Wood AW, Voisin N, et al (2004) The Effects of Climate Change on the Hydrology and Water Resources of the Colorado River Basin. Clim Change 62:337–363. doi: 10.1023/B:CLIM.0000013684.13621.1f

Dickinson RE, Henderson-Sellers A, Kennedy PJ (1993) Biosphere-Atmosphere Transfer Scheme (BATS) Version le as Coupled to the NCAR Community Climate Model. NCAR Technical Note, NCAR/TN-387+STR.

Döll, P. and Fiedler, K.: Global-scale modeling of groundwater recharge, Hydrol. Earth Syst. Sci., 12(3), 863–885, doi:10.5194/hess-12-863-2008, 2008.

Döll, P.: Vulnerability to the impact of climate change on renewable groundwater resources: A global-scale assessment, Environ. Res. Lett., 4(3), doi:10.1088/1748-9326/4/3/035006, 2009.

Dumanski, S., Pomeroy, J. W. and Westbrook, C. J.: Hydrological regime changes in a Canadian Prairie basin, Hydrol. Process., 29(18), 3893–3904, doi:10.1002/hyp.10567, 2015.

Environment Canada: Municipal Water Use, 2009 Statistics, 2011 Munic. Water Use Rep., 24, doi:En11-2/2009E-PDF Information, 2011.

Fan Y, Miguez-Macho G, Weaver CP, et al (2007) Incorporating water table dynamics in climate modeling: 1. Water table observations and equilibrium water table simulations. J Geophys Res Atmos 112:1–17. doi: 10.1029/2006JD008111

Fan, Y., Li, H. and Miguez-Macho, G.: Global patterns of groundwater table depth, Science (80-.)., 339(6122), 940–943, doi:10.1126/science.1229881, 2013.

Fan, Y.: Groundwater in the Earth's critical zones: Relevance to large-scale patterns and processes, Water Resour. Res., 3052–3069, doi:10.1002/2015WR017037.Received, 2015.

Granger RJ, Gray DM: Evaporation from natural non-saturated surface. J. Hydrol., 111, 21–29, 1989.

Gray DM: Handbook on the Principles of Hydrology: With Special Emphasis Directed to Canadian Conditions in the Discussion, Applications, and Presentation of Data. Water Information Center: Huntingdon, New York, 1970. ISBN:0-912394-07-2

Green, T. R., Taniguchi, M., Kooi, H., Gurdak, J. J., Allen, D. M., Hiscock, K. M., Treidel, H. and Aureli, A.: Beneath the surface of global change: Impacts of climate change on groundwater, J. Hydrol., 405(3–4), 532–560, doi:10.1016/j.jhydrol.2011.05.002, 2011.

Hayashi, M., Van Der Kamp, G. and Schmidt, R.: Focused infiltration of snowmelt water in partially frozen soil under small depressions, J. Hydrol., 270(3–4), 214–229, doi:10.1016/S0022-1694(02)00287-1, 2003.

Hayashi, M., van der Kamp, G. and Rosenberry, D. O.: Hydrology of Prairie Wetlands: Understanding the Integrated Surface-Water and Groundwater Processes, Wetlands, 36, 237–254, doi:10.1007/s13157-016-0797-9, 2016.

Ireson, A. M., van der Kamp, G., Ferguson, G., Nachshon, U. and Wheater, H. S.: Hydrogeological processes in seasonally frozen northern latitudes: understanding, gaps and challenges, Hydrogeol. J., 21(1), 53–66, doi:10.1007/s10040-012-0916-5, 2013.

Ireson, A. M., Barr, A. G., Johnstone, J. F., Mamet, S. D., van der Kamp, G., Whitfield, C. J., Michel, N. L., North, R. L., Westbrook, C. J., DeBeer, C., Chun, K. P., Nazemi, A. and Sagin, J.: The changing water cycle: the Boreal Plains ecozone of Western Canada, Wiley Interdiscip. Rev. Water, 2(5), 505–521, doi:10.1002/wat2.1098, 2015.

Johnson, W. C., Werner, B., Guntenspergen, G. R., Voldseth, R. A., Millett, B., Naugle, D. E., Tulbure, M., Carroll, R. W. H., Tracy, J. and Olawsky, C.: Prairie Wetland Complexes as Landscape Functional Units in a Changing Climate, Bioscience, 60(2), 128–140, doi:10.1525/bio.2010.60.2.7, 2010.

Kelln C, Barbour L, Qualizza C (2007) Preferential Flow in a Reclamation Cover : Hydrological and Geochemical Response. 1277–1289

Koren, V., Schaake, J., Mitchell, K., Duan, Q.-Y., Chen, F., & Baker, J. M. (1999). A parameterization of snowpack and frozen ground intended for NCEP weather and climate models. Journal of Geophysical Research: Atmospheres, 104(D16), 19569–19585. https://doi.org/10.1029/1999JD900232

Koster, R. D., Dirmeyer, P. A., Guo, Z., Bonan, G., Chan, E., Cox, P., Gordon, C. T., Kanae, S., Kowalczyk, E., Lawrence, D., Liu, P., Lu, C.-H., Malyshev, S., McAvaney, B., Mitchell, K., Mocko, D., Oki, T., Oleson, K., Pitman, A., Sud, Y. C., Taylor, C. M., Verseghy, D., Vasic, R., Xue, Y. and Yamada, T.: Regions of Strong Coupling Between Soil Moisture and Precipitation, Science (80-.)., 305(5687), 1138 LP-1140 [online] Available from: http://science.sciencemag.org/content/305/5687/1138.abstract, 2004.

Kollet SJ, Maxwell RM (2008) Capturing the influence of groundwater dynamics on land surface processes using an integrated, distributed watershed model. Water Resour Res 44:1–18. doi: 10.1029/2007WR006004

Kurylyk, B. L. and MacQuarrie, K. T. B.: The uncertainty associated with estimating future groundwater recharge: A summary of recent research and an example from a small unconfined aquifer in a northern humid-continental climate, J. Hydrol., 492, 244–253, doi:10.1016/j.jhydrol.2013.03.043, 2013.

Liu, C., Ikeda, K., Rasmussen, R., Barlage, M., Newman, A. J., Prein, A. F., Chen, F., Chen, L., Clark, M., Dai, A., Dudhia, J., Eidhammer, T., Gochis, D., Gutmann, E., Kurkute, S., Li, Y., Thompson, G. and Yates, D.: Continental-scale convection-permitting modeling of the current and future climate of North America, Clim. Dyn., 49(1–2), 71–95, doi:10.1007/s00382-016-3327-9, 2017.

Martinez, J. A., Dominguez, F. and Miguez-Macho, G.: Effects of a Groundwater Scheme on the Simulation of Soil Moisture and Evapotranspiration over Southern South America, J. Hydrometeorol., 17(11), 2941–2957, doi:10.1175/JHM-D-16-0051.1, 2016.

Maxwell RM, Miller NL (2005) Development of a Coupled Land Surface and Groundwater Model. 233–247

Maxwell, R. M. and Kollet, S. J.: Interdependence of groundwater dynamics and land-energy feedbacks under climate change, Nat. Geosci., 1(10), 665–669, doi:10.1038/ngeo315, 2008.

Maxwell, R. M., Condon, L. E. and Kollet, S. J.: A high-resolution simulation of groundwater and surface water over most of the continental US with the integrated hydrologic model ParFlow v3, Geosci. Model Dev., 8(3), 923–937, doi:10.5194/gmd-8-923-2015, 2015.

Meixner, T., Manning, A. H., Stonestrom, D. A., Allen, D. M., Ajami, H., Blasch, K. W., Brookfield, A. E., Castro, C. L., Clark, J. F., Gochis, D. J., Flint, A. L., Neff, K. L., Niraula, R., Rodell, M., Scanlon, B. R., Singha, K. and Walvoord, M. A.: Implications of projected climate change for groundwater recharge in the western United States, J. Hydrol., 534, 124–138, doi:10.1016/j.jhydrol.2015.12.027, 2016.

Miguez-Macho, G., Fan, Y., Weaver, C. P., Walko, R. and Robock, A.: Incorporating water table dynamics in climate modeling: 2. Formulation, validation, and soil moisture simulation, J.

Miguez-Macho, G. and Fan, Y.: The role of groundwater in the Amazon water cycle: 1. Influence on seasonal streamflow, flooding and wetlands, J. Geophys. Res. Atmos., 117(15), 1–30, doi:10.1029/2012JD017539, 2012.

Moeck, C., Brunner, P. and Hunkeler, D.: The influence of model structure on groundwater recharge rates in climate-change impact studies, Hydrogeol. J., 24(5), 1171–1184, doi:10.1007/s10040-016-1367-1, 2016.

Mohammed, A. A., Kurylyk, B. L., Cey, E. E. and Hayashi, M.: Snowmelt Infiltration and Macropore Flow in Frozen Soils: Overview, Knowledge Gaps, and a Conceptual Framework, Vadose Zo. J., 17(1), doi:10.2136/vzj2018.04.0084, 2018.

Musselman, K. N., Clark, M. P., Liu, C., Ikeda, K. and Rasmussen, R.: Slower snowmelt in a warmer world, Nat. Clim. Chang., 7(February), 214–220, doi:10.1038/NCLIMATE3225, 2017.

National Research Council: Groundwater fluxes across inter- faces. The National Academy Press, 85 pp, 2003

Niraula R, Meixner T, Dominguez F, et al (2017) How Might Recharge Change Under Projected Climate Change in the Western U.S.? Geophys Res Lett 44:10,407-10,418. doi: 10.1002/2017GL075421

Niu, G.-Y., & Yang, Z.-L. (2006). Effects of Frozen Soil on Snowmelt Runoff and Soil Water Storage at a Continental Scale. Journal of Hydrometeorology, 7(5), 937–952. https://doi.org/10.1175/JHM538.1

Niu G, Yang Z, Dickinson RE, Gulden LE (2007) Development of a simple groundwater model for use in climate models and evaluation with Gravity Recovery and Climate Experiment data. 112:1–14. doi: 10.1029/2006JD007522

Niu, G. Y., Yang, Z. L., Mitchell, K. E., Chen, F., Ek, M. B., Barlage, M., Kumar, A., Manning, K., Niyogi, D., Rosero, E., Tewari, M. and Xia, Y.: The community Noah land surface model with multiparameterization options (Noah-MP): 1. Model description and evaluation with local-scale measurements, J. Geophys. Res. Atmos., 116(12), 1–19, doi:10.1029/2010JD015139, 2011.

Niu G-Y, Zeng X (2012) Earth System Model, Modeling the Land Component of. In: Climate Change Modeling Methodology. Springer New York, New York, NY, pp 139–168

Pokhrel, Y. N., Fan, Y., Miguez-Macho, G., Yeh, P. J. F. and Han, S. C.: The role of groundwater in the Amazon water cycle: 3. Influence on terrestrial water storage computations and comparison with GRACE, J. Geophys. Res. Atmos., 118(8), 3233–3244, doi:10.1002/jgrd.50335, 2013.

Pokhrel, Y. N., Fan, Y. and Miguez-Macho, G.: Potential hydrologic changes in the Amazon by the end of the 21st century and the groundwater buffer, Environ. Res. Lett., 9(8), doi:10.1088/1748-9326/9/8/084004, 2014.

Pomeroy, J. W.: The cold regions hydrological model: a platform for basing process representation and model structure on physical evidence, Hydrol. Process., 21, 2650–2667, doi:10.1002/hyp, 2007.

Prein, A. F., Gobiet, A., Suklitsch, M., Truhetz, H., Awan, N. K., Keuler, K. and Georgievski, G.: Added value of convection permitting seasonal simulations, , 2655–2677, doi:10.1007/s00382-013-1744-6, 2013.

Prein, A. F., Langhans, W., Fosser, G., Ferrone, A., Ban, N., Goergen, K., Keller, M., Tölle, M., Gutjahr, O., Feser, F., Brisson, E., Kollet, S., Schmidli, J., Van Lipzig, N. P. M. and Leung, R.: A review on regional convection-permitting climate modeling: Demonstrations, prospects, and challenges, Rev. Geophys., 53(2), 323–361, doi:10.1002/2014RG000475, 2015.

Rasmussen, K. L., Prein, A. F., Rasmussen, R. M., Ikeda, K. and Liu, C.: Changes in the convective population and thermodynamic environments in convection-permitting regional climate simulations over the United States, Clim. Dyn., (0123456789), 1–26, doi:10.1007/s00382-017-4000-7, 2017.

Remenda VH, van der Kamp G, Cherry JA (1996) Use of vertical profiles of • 180 to constrain estimates of hydraulic conductivity in a thick, unfractured aquitard. 32:2979–2987

Shangguan W, Dai Y, Duan Q, et al (2014) Journal of Advances in Modeling Earth Systems. J Adv Model Earth Syst 6:249–263. doi: 10.1002/2013MS000293.Received

Sherwood, S. C., Bony, S. and Dufresne, J.: Spread in model climate sensitivity traced to atmospheric convective mixing, , doi:10.1038/nature12829, 2014.

Siebert, S., Burke, J., Faures, J. M., Frenken, K., Hoogeveen, J., Döll, P. and Portmann, F. T.: Groundwater use for irrigation - A global inventory, Hydrol. Earth Syst. Sci., 14(10), 1863–1880, doi:10.5194/hess-14-1863-2010, 2010.

Smerdon, B. D.: A synopsis of climate change effects on groundwater recharge, J. Hydrol., 555, 125–128, doi:10.1016/j.jhydrol.2017.09.047, 2017.

Statistics Canada: Quarterly Estimates of the Population of Canada, the Provinces and the Territories, 11-3, Catalogue 91-001, Ottawa, 1996

Taylor, R. G.: Ground water and climate change, , 3(November 2012), doi:10.1038/NCLIMATE1744, 2013.

Tremblay, L., Larocque, M., Anctil, F. and Rivard, C.: Teleconnections and interannual variability in Canadian groundwater levels, J. Hydrol., 410(3–4), 178–188, doi:10.1016/j.jhydrol.2011.09.013, 2011.

UNESCO: Groundwater Resources of the Wrold and Their Use, edited by I. Zektser and L. Everett, Paris., 2004.

Van Der Kamp G, Hayashi M (2009) Groundwater-wetland ecosystem interaction in the semiarid glaciated plains of North America. Hydrogeol J 17:203–214. doi: 10.1007/s10040-008-0367-1

Xue Y, Sellers PJ, Kinter JL, Shukla J (1991) A Simplified Biosphere Model for Global Climate Studies. J Clim 4:345–364. doi: 10.1175/1520-0442(1991)004<0345:ASBMFG>2.0.CO;2

Yang, Z. L., Niu, G. Y., Mitchell, K. E., Chen, F., Ek, M. B., Barlage, M., Longuevergne, L., Manning, K., Niyogi, D., Tewari, M. and Xia, Y.: The community Noah land surface model with multiparameterization options (Noah-MP): 2. Evaluation over global river basins, J. Geophys. Res. Atmos., 116(12), 1–16, doi:10.1029/2010JD015140, 2011.

Table and Figure

Table 1. Summary of the locations and aquifer type and soil type of the 33 selected wells.

Site Name/ Site No.	Lat	Lon	Elev	Aquifer type	Aquifer Lithology	Model Elevation	Model Soil type
Devon 0162	53.41	-113.76	700.0	Unconfined	Sand	697.366	Sandy loam
Hardisty 0143	52.67	-111.31	622.0	Unconfined	Gravel	633.079	Loam
Kirkpatrick Lake 0229	51.95	-111.44	744.5	Semi-confined	Sandstone	778.311	Sandy loam
Metiskow 0267	52.42	-110.60	677.5	Unconfined	Sand	679.516	Loamy sand
Wagner 0172	53.56	-113.82	670.0	Surficial	Sand	670.845	Silt loam
Narrow Lake 252	54.60	-113.63	640.0	Unconfined	Sand	701.0	Clay loam
Baildon 060	50.25	-105.50	590.184	Surficial	-	580.890	Sandy loam
Beauval	55.11	-107.74	434.3	Intertill	Sand	446.5	Sandy loam
Blucher	52.03	-106.20	521.061	Intertill	Sand/Gravel	523.217	Loam
Crater Lake	50.95	-102.46	524.158	Intertill	Sand/Gravel/Clay	522.767	Loam
Duck Lake	52.92	-106.23	502.920	Surficial	Sand	501.729	Loamy sand
Forget	49.70	-102.85	606.552	Surficial	Sand	605.915	Sandy loam
Garden Head	49.74	-108.52	899.160	Bedrock	Sand/Till	894.357	Clay loam
Nokomis	51.51	-105.06	516.267	Bedrock	Sand	511.767	Clay loam
Shaunavon	49.69	-108.50	896.040	Bedrock	Sand/Till	900.433	Clay loam
Simpson 13	51.45	-105.18	496.620	Surficial	Sand	493.313	Sandy loam
Simpson 14	51.457	-105.19	496.600	Surficial	Sand	493.313	Sandy loam
Yorkton 517	51.17	-102.50	513.643	Surficial	Sand/Gravel	511.181	Loam
Agrium 43	52.03	-107.01	500.229	Intertill	Sand	510.771	Loam
460120097591803	46.02	-97.98	401.177	Alluvial	Sand/Gravel	400.381	Sandy loam
461838097553402	46.31	-97.92	401.168	-	Sand/Gravel	404.719	Clay loam
462400097552502	46.39	-97.92	409.73	-	Sand/Gravel	407.405	Sandy loam
462633097163402	46.44	-97.27	325.52	Alluvial	Sand/Gravel	323.728	Sandy loam
463422097115602	46.57	-97.19	320.40	Alluvial	Sand/Gravel	314.167	Sandy loam
464540100222101	46.76	-100.37	524.91	-	Sand/Gravel	522.600	Clay loam
473841096153101	47.64	-96.25	351.77	Surficial	Sand/Gravel	344.180	Loamy sand
473945096202402	47.66	-96.34	327.78	Surficial	Sand/Gravel	328.129	Sandy loam
474135096203001	47.69	-96.34	325.97	Surficial	Sand/Gravel	327.764	Sandy loam
474436096140801	47.74	-96.23	341.90	Surficial	Sand/Gravel	336.210	Sandy loam
475224098443202	47.87	-98.74	451.33	-	Sand/Gravel	450.463	Sandy loam
481841097490301	48.31	-97.81	355.61	-	Sand/Gravel	359.568	Clay loam
482212099475801	48.37	-99.79	488.65	-	Sand/Gravel	488.022	Sandy loam
CRN Well WLN03	45.98	-95.20	410.7	Surficial	Sand/Gravel	411.4	Sandy loam

Table 2. Summary of mean and standard deviation (std) of WTD from 33 groundwater wells, from observation records (OBS), default model (CTRL) and replacing with sand soil simulation (REP). Bold texts indicate improvement in the REP than the CTRL run.

Site Name/Number	OBS_mean	CTRL_mean	REP_mean	OBS_std	CTRL_std	REP std
Devon 0162	-2.46	-2.69	**-2.38**	0.43	0.45	0.09
Hardisty 0143	-2.44	-8.91	**-6.88**	0.41	0.64	**0.36**
Kirkpatrick Lake 0229	-4.22	-4.03	-3.45	0.43	0.98	**0.22**
Metiskow 0267	-2.54	-5.39	**-4.43**	0.34	0.78	**0.55**
Narrow Lake 252	-2.31	-4.81	**-3.75**	0.28	0.60	0.51
Wagner 0172	-2.14	-8.06	**-2.70**	0.48	0.37	0.21
Baildon 060	-2.80	-3.29	**-3.20**	0.47	0.58	0.30
Beauval	-3.78	-4.85	**-4.20**	0.44	0.56	0.32
Blucher	-2.20	-4.24	**-2.16**	0.3	0.92	**0.26**
Crater Lake	-4.33	-3.97	-3.64	1.1	0.4	0.28
Duck Lake	-3.65	-3.69	-3.17	0.54	0.41	**0.62**
Forget	-2.28	-2.37	**-2.23**	0.33	0.17	0.19
Garden Head	-3.67	-4.85	**-3.77**	0.88	0.70	0.30
Nokomis	-1.04	-2.70	**-2.17**	0.23	0.55	**0.17**
Shaunavon	-1.62	-4.41	**-2.58**	0.42	0.69	0.20
Simpson 13	-4.82	-4.83	-3.02	0.31	0.91	**0.17**
Simpson 14	-2.03	-2.61	**-1.82**	0.34	0.18	**0.27**
Yorkton 517	-2.87	-3.97	**-1.98**	0.8	0.46	0.32
Agrium 43	-2.66	-3.75	**-3.38**	0.32	1.05	**0.36**
460120097591803	-1.44	-2.33	**-1.63**	0.56	0.24	**0.50**
461838097553402	-1.17	-2.32	**-1.68**	0.27	0.24	0.43
462400097552502	-4.9	-5.61	**-5.37**	0.29	0.09	**0.17**
462633097163402	-1.18	-1.49	**-1.02**	0.46	0.29	**0.54**
463422097115602	-1.36	-2.28	**-1.66**	0.34	0.23	0.49
464540100222101	-2.02	-3.64	**-2.78**	0.52	0.43	0.32
473841096153101	-0.77	-1.48	**-1.37**	0.24	0.18	0.51
473945096202402	-1.59	-1.58	-1.56	0.32	0.24	0.51
474135096203001	-0.72	-1.48	**-1.30**	0.33	0.25	0.54
474436096140801	-2.44	-2.29	-1.96	0.39	0.21	**0.40**
475224098443202	-4.52	-4.28	-5.31	0.75	0.52	0.34
481841097490301	-4.39	-4.24	-4.58	0.79	0.28	0.17
482212099475801	-2.13	-2.32	**-2.26**	0.24	0.20	0.17
CRN WLN 03	-2.04	-2.18	-1.88	0.24	0.18	0.43

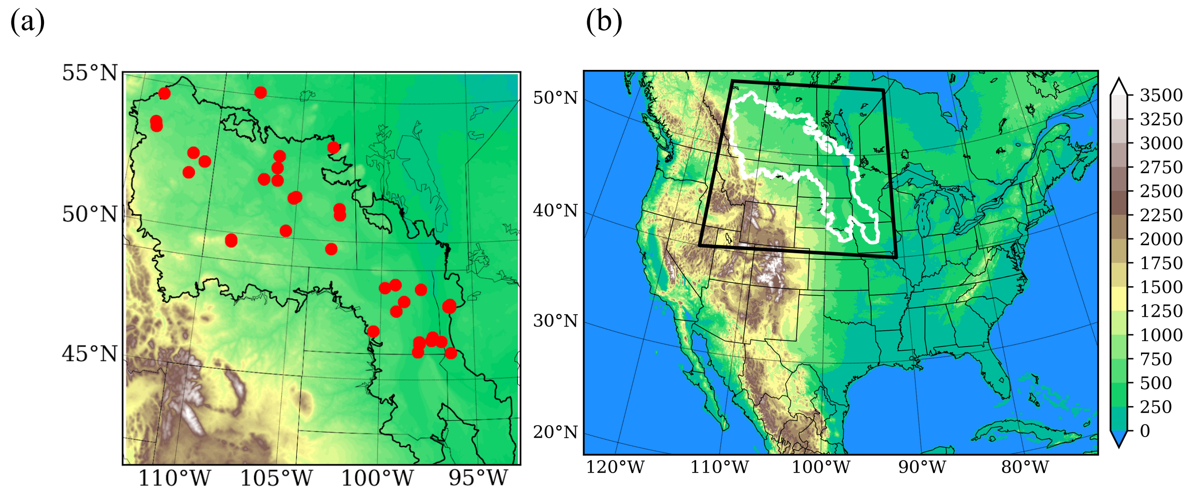

Fig. 1 (a) Topography of the Prairie Pothole Region (PPR; black outline) and groundwater wells (red dots); (b) Topography of the WRF CONUS domain, the black box indicates the PPR domain.

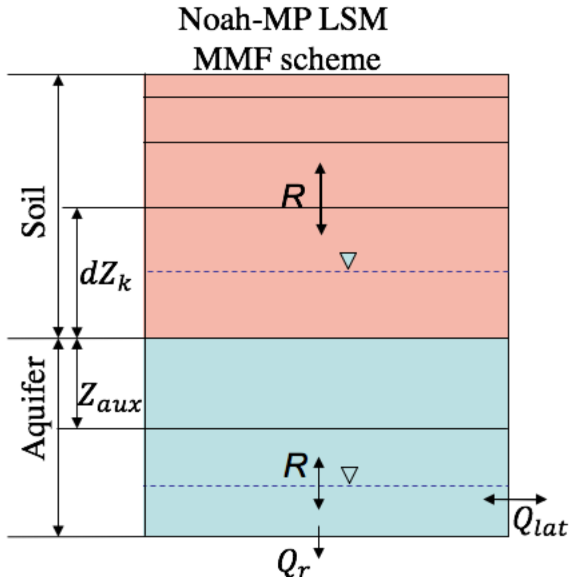

Fig. 2 Structure of the Noah-MP LSM coupled with MMF groundwater scheme, the top 2-m soil of 4 layers whose thicknesses are 0.1, 0.3, 0.6 and 1.0 m. An unconfined aquifer is added below the 2-m boundary, including an auxiliary layer and the saturated aquifer. Positive flux of *R* denotes downward flow. Two water tables are shown, one within the 2-m soil and one below, indicating that the model is capable to deal with both shallow and deep water table.

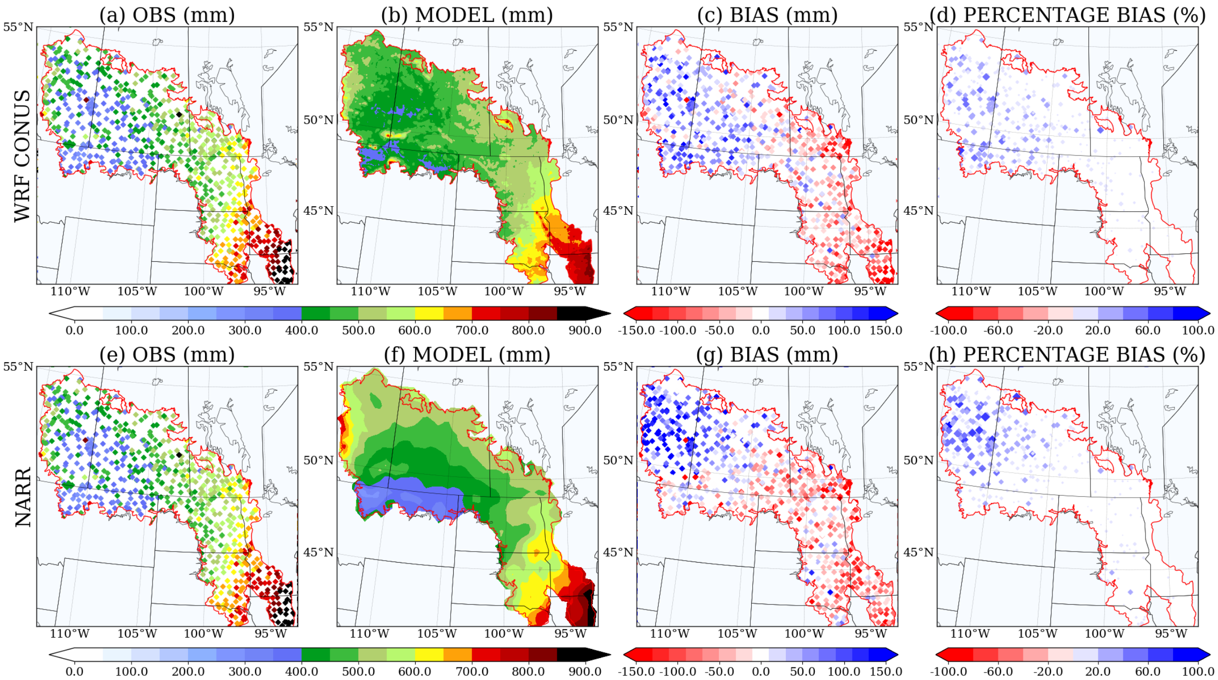

Fig. 3 Evaluation of the annual precipitation from two model products (b, f), WRF CONUS and NARR against rain gauge observation (a, e), their bias (c, g) and percentage bias (d, h).

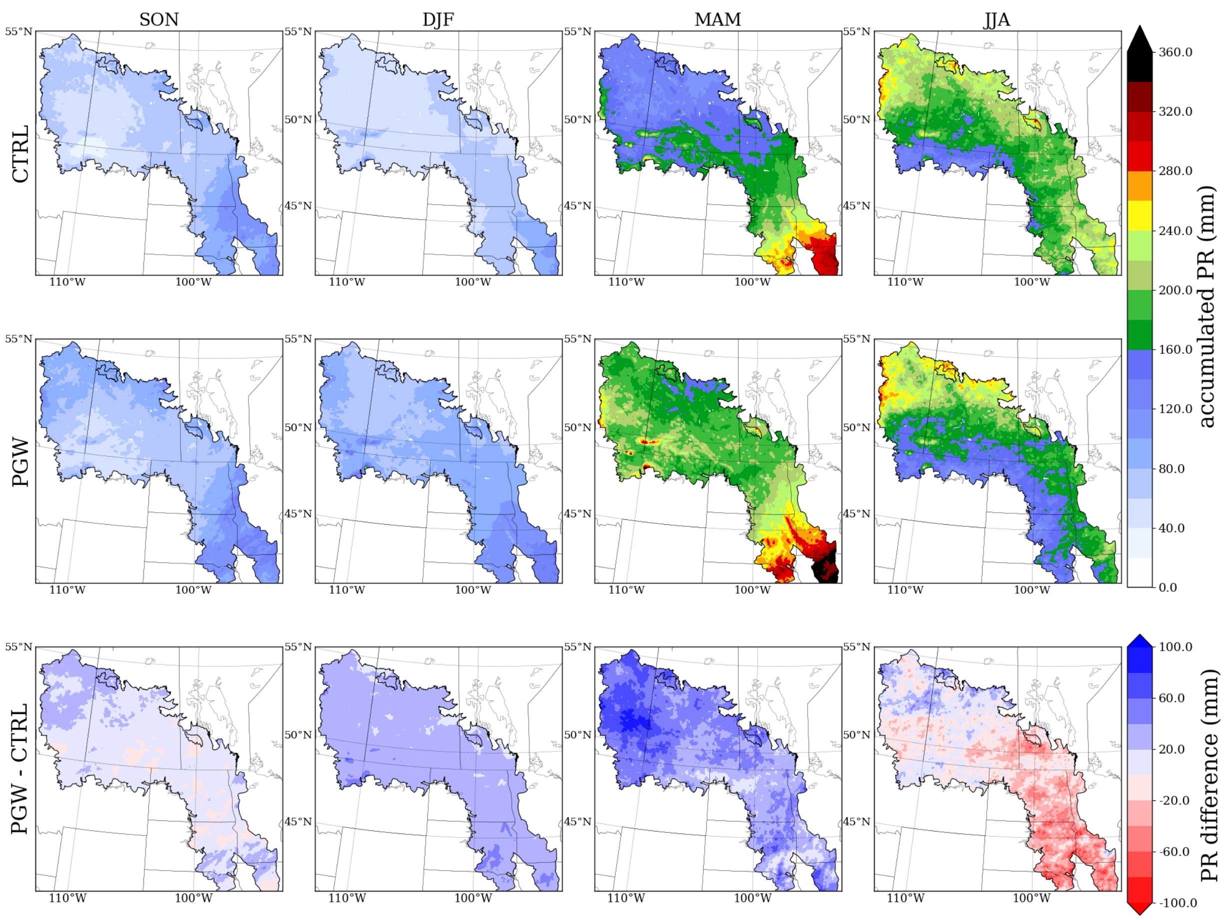

Fig. 4 Seasonal Accumulated precipitation from current climate (CTRL, top), future climate (PGW, middle) and projected change (PGW-CTRL, bottom) in forcing data.

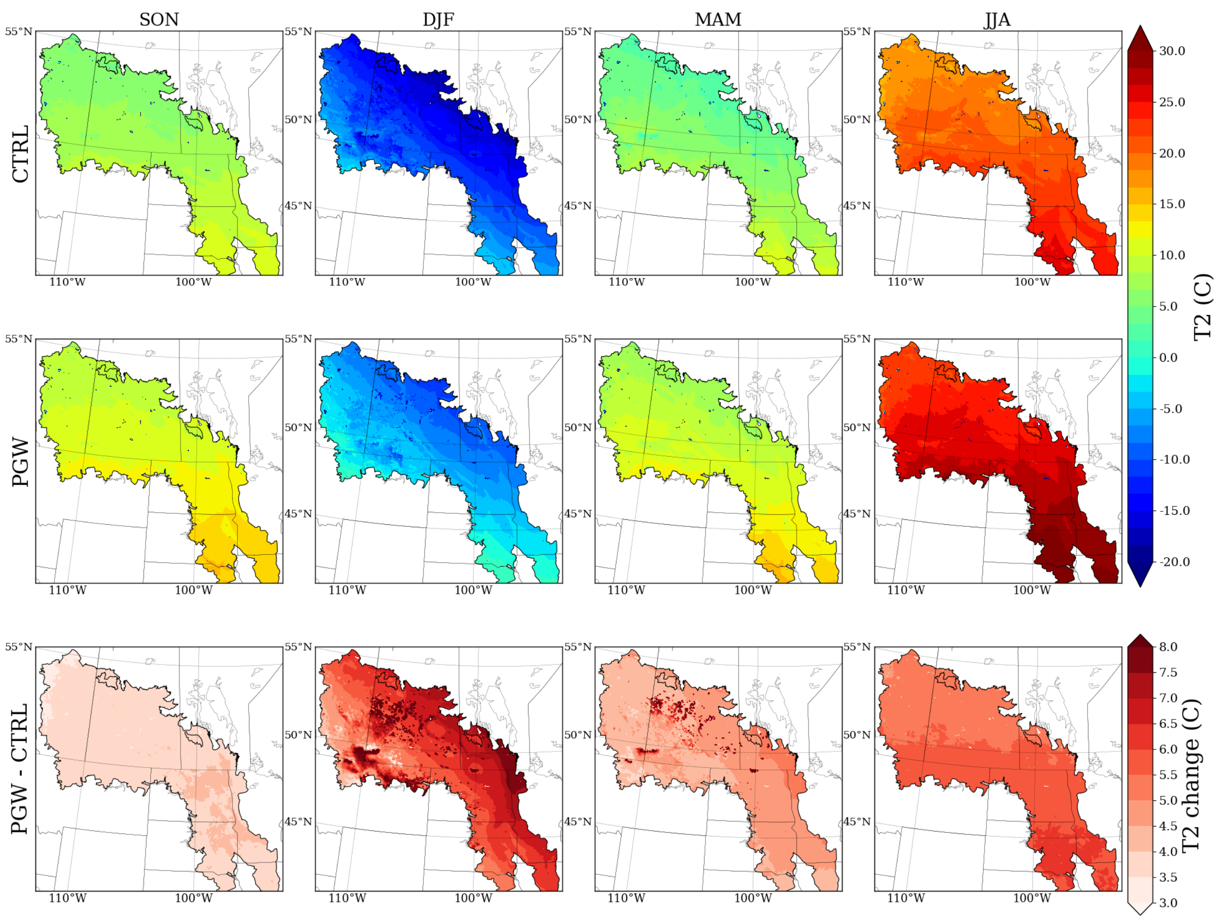

Fig. 5 Seasonal temperatures from current climate (CTRL, top), future climate (PGW, middle) and projected change (PGW-CTRL, bottom) in forcing data.

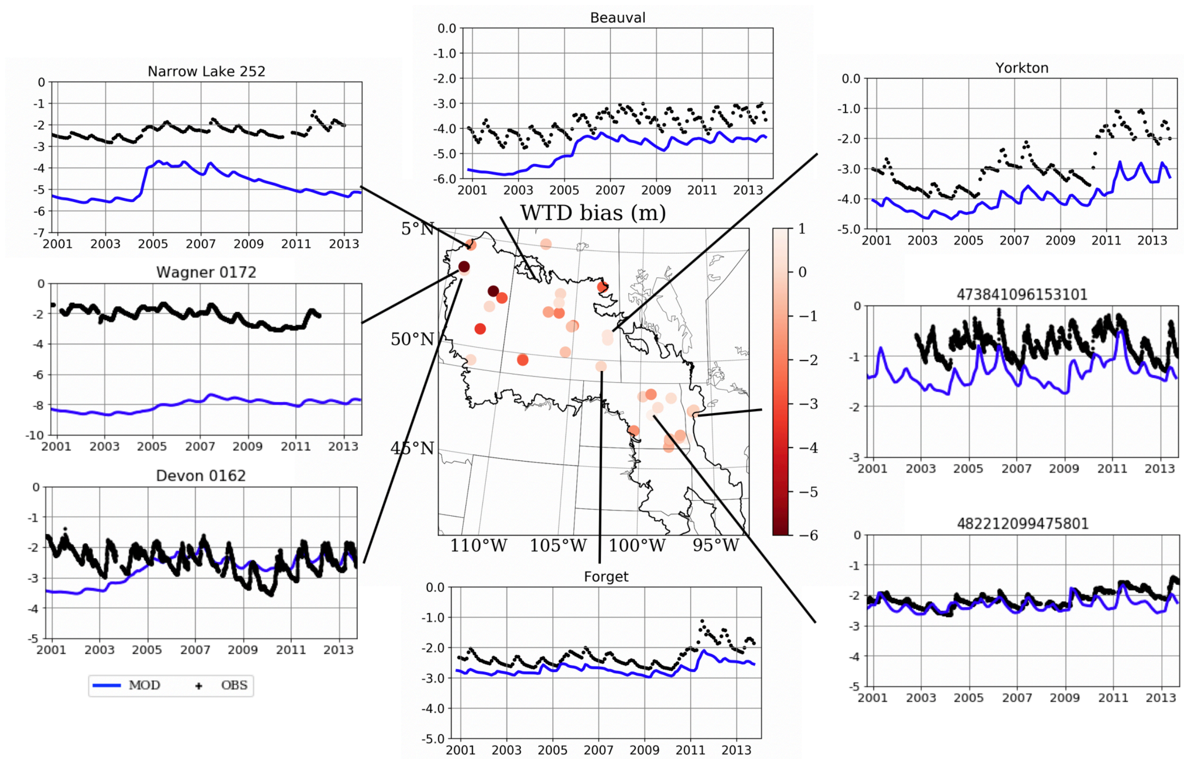

Fig. 6. WTD (m) bias from CTRL simulation and timeseries from 8 groundwater wells in PPR (black for observation and blue for CTRL model simulation). See Table 2 CTRL column for the model statistics and supplemental materials for complete timeseries from 33 wells.

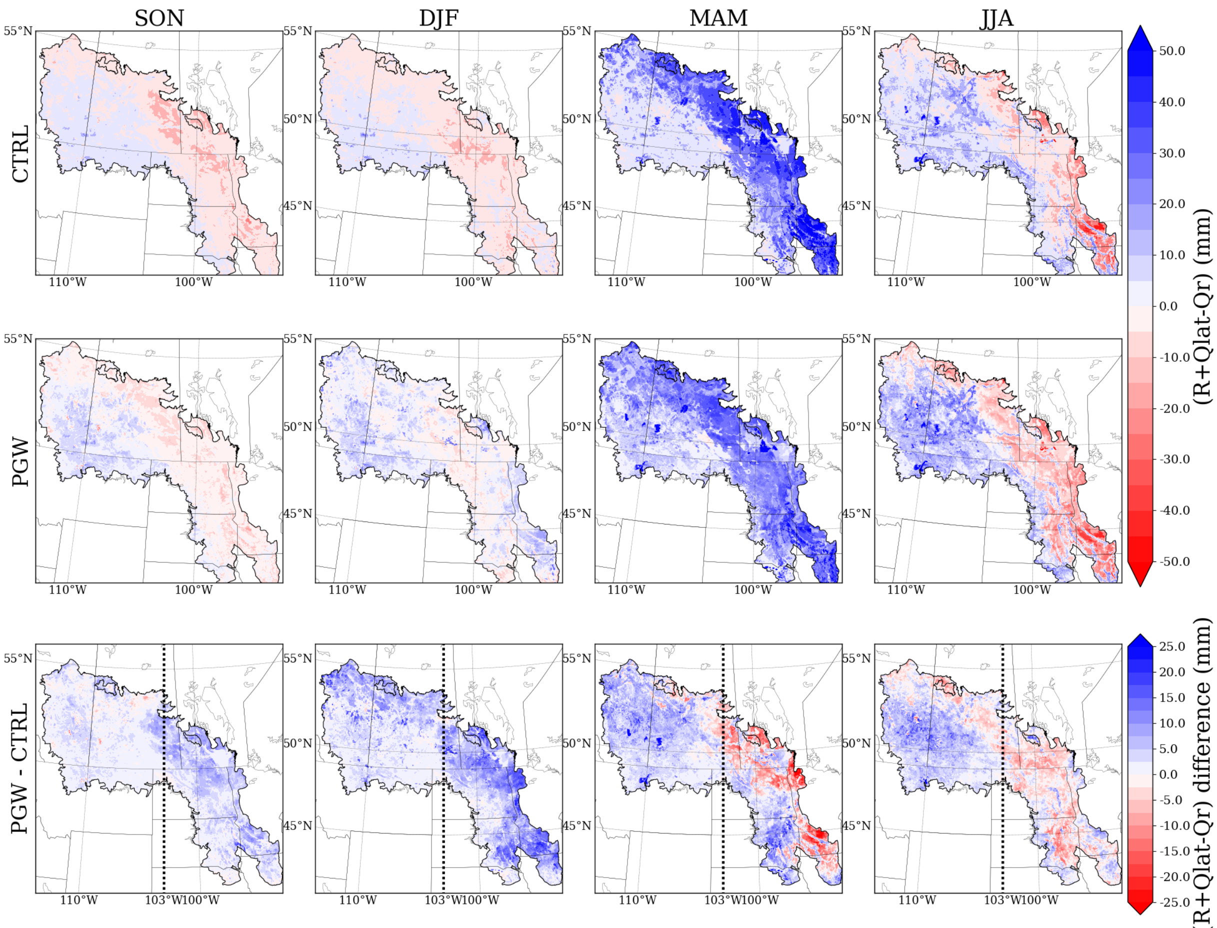

Fig. 7 Seasonal accumulated total groundwater fluxes (R+$Q_{lat} - Q_r$) for current climate (CTRL, top), future climate (PGW, middle) and projected change (PGW-CTRL, bottom) in forcing data. Black dashed lines in PGW-CTRL separate the PPR into eastern and western halves.

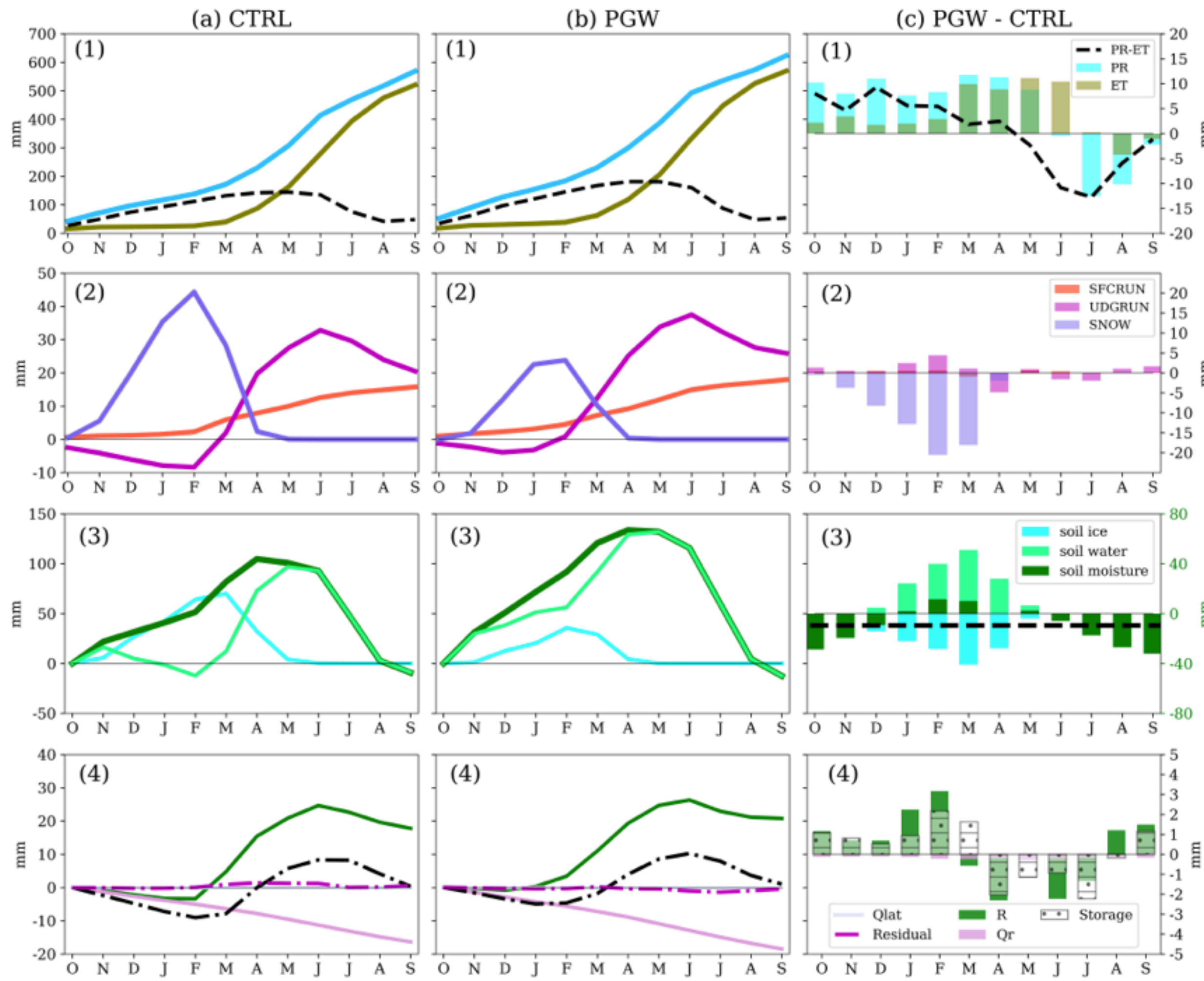

storage change: 1.763 mm
recharge change: 4.152 mm
river flux change: 2.260 mm
lateral flux change: -0.001 mm

Fig. 8 Water budget analysis in the **eastern PPR** in (a) CTRL, (b) PGW and (c) PGW – CTRL. Water budget terms include: (1) *PR & ET*, (2) surface snow, surface runoff and underground runoff (*SNOW*, *SFCRUN*, and *UDGRUN*), (3) change of soil moisture storage (soil water, soil ice and total soil moisture, ΔSMC) and (4) groundwater fluxes and the change of groundwater storage (R, Q_{lat}, Q_r, ΔS_g). The annual mean soil moisture change (PGW-CTRL) is shown with black dashed line in (3). The Residual term is defined as $Res = (R+Q_{lat}-Q_r)-\Delta S_g$ in (4). Note that in (a) and (b) the accumulated fluxes and change in storage are shown in lines, whereas in (c) the difference in (PGW-CTRL) is shown for each individual month in bars.

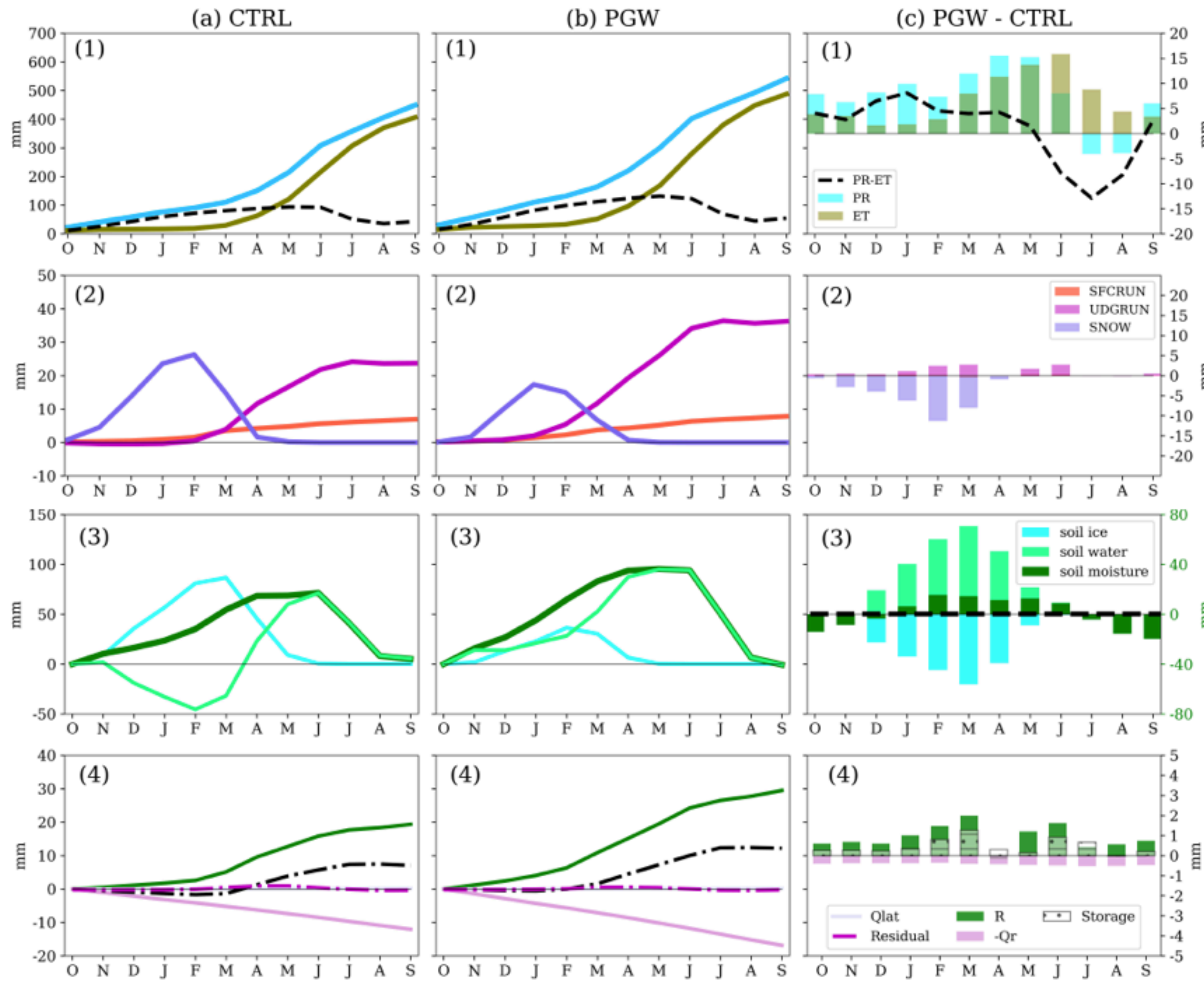

storage change: 5.390 mm
recharge change: 10.727 mm
river flux change: 5.207 mm
lateral flux change: 0.000 mm

Fig. 9 Same as Fig. 8. Water budget analysis in the **western PPR**: in (a) CTRL, (b) PGW and (c) PGW – CTRL. Water budget terms include: (1) *PR & ET*, (2) surface snow, surface runoff and underground runoff (*SNOW*, *SFCRUN*, and *UDGRUN*), (3) change of soil moisture storage (soil water, soil ice and total soil moisture, ΔSMC) and (4) groundwater fluxes and the change of groundwater storage (R, Q_{lat}, Q_r, ΔS_g). The annual mean soil moisture change (PGW-CTRL) is shown with black dashed line in (3). The Residual term is defined as $Res = (R+Q_{lat}-Q_r)-\Delta S_g$ in (4). Note that in (a) and (b) the accumulated fluxes and change in storage are shown in lines, whereas in (c) the difference in (PGW-CTRL) is shown for each individual month in bars.

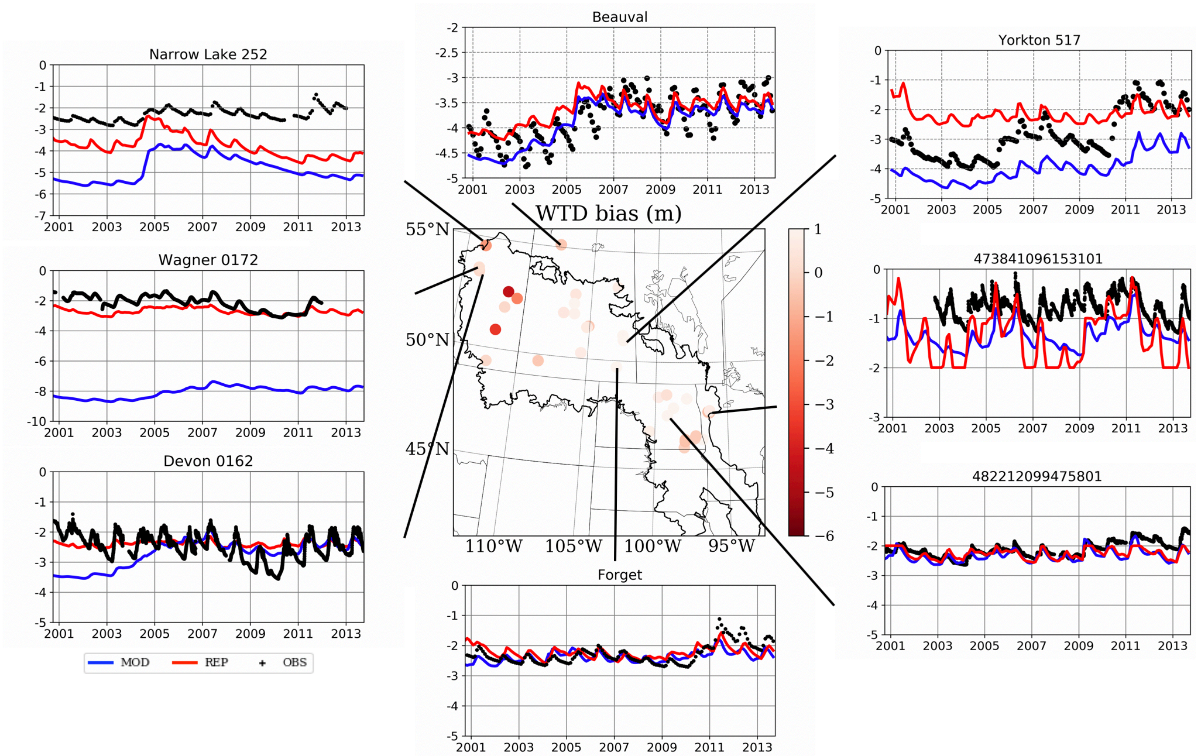

Fig. 10 Same as Fig. 6, WTD (m) bias from CTRL simulation and timeseries from 8 groundwater wells in PPR (black for observation and blue for CTRL model simulation, and red for the replacing soil type simulation). REP is the additional simulation by replacing the default soil type in the model with sandy soil type.